comparison between the experimental and calculated relative proton affinity is reasonable.

In both of these computational studies it was found that inclusion of d orbitals did not significantly change the relative proton affinity values. It was thus concluded that stabilization is not a result of delocalization into empty Si d orbitals. Evidence such as increased Si–H bond lengths in the silylmethyl anion (compared to those in the neutral molecule, CH_3SiH_3) suggested hyperconjugation between negatively charged carbon and the adjacent silyl group could be responsible for the stabilization.

Hyperconjugative interactions in α-silyl-substituted carbanions are possible because of the electropositive nature of Si. The Si–H bonds in CH_3SiH_3 are polarized, with electron density predominantly on the H atoms.[32] The coefficients are large on H in the bonding orbitals and therefore large on Si in the antibonding orbitals. Electron donation from the p-type highest occupied molecular orbital (HOMO) of the carbanion into the Si–H antibonding orbital, represented pictorially in Figure 2, is possible because of the large amount of overlap and the similarity in energetics and symmetry between the orbitals involved.

Mixing of lone-pair anionic electrons with nearby antibonding orbitals is especially favorable because of the unusually high energy of the anion. Such mixing has been shown to be responsible for the stabilization of alkoxide anions by large alkyl groups.[33]

Experiments[34] and calculations[35a] indicate that second-row substituents are more effective at stabilizing carbanions than those of the first row. The electron affinity and acidity measurements in this study complete the series of data available for second-row α-heteroatom methyl anions (XCH_2^-). Table II lists the relative proton affinities (again, relative to methyl anion) of α-substituted methyl anions obtained from experiments. Listed beneath each experimental value is a calculated relative proton affinity, for comparison. The systems being compared are not identical; nevertheless, agreement in magnitude and the second-row trend is shown.

The relative proton affinities indicate that silicon is most effective at stabilizing a carbanion. All of the second-row substituents, however, considerably stabilize methyl anion. Hyperconjugation and polarization arguments have been similarly invoked to rationalize carbanion stabilization by α-P and -S substituents.[35]

Interestingly, an α-silyl substituent does not appreciably stabilize a carbon radical. This had been noted previously, based on the results of bond dissociation energy measurements[36] and gas kinetic studies of organosilane pyrolysis,[37] indicating an α-silyl stabilization of only 1 kcal/mol. This is probably a consequence of the relative energetics of the radical center and the adjacent bonding and antibonding orbitals. Again in analogy to alkoxyl radicals,[33] the energy of the radical center is such that mixing with both the bonding (destabilizing interaction) and antibonding (stabilizing interaction) orbitals occurs, resulting in no net stabilization. The HOMO in the carbanion is closer in energy to the Si–H antibonding orbitals, such that mixing with these orbitals predominates.

Conclusions

We have measured the electron photodetachment spectrum of the (trimethylsilyl)methyl anion, from which we have determined the electron affinity of the corresponding neutral radical and the acidity of the conjugate acid. Comparison of these thermochemical data to those known for methyl radical (methane) gives a direct, quantitative measure of α-silyl stabilization. The stabilization energy is large in magnitude and in good agreement with previous quantum calculations.

Acknowledgment. We are grateful for support from the National Science Foundation and materials made available by the San Francisco Laser Center, supported by the National Science Foundation.

Registry No. 1, 88036-00-4; $Me_3SiCH_3^{\bullet}$, 19469-02-4.

(32) (a) Liskow, D. H.; Schaefer, H. F., III *J. Am. Chem. Soc.* **1972**, *94*, 6641. (b) Wiberg, K. B.; Wendoloski, J. J. *J. Phys. Chem.* **1984**, *88*, 586.
(33) (a) Hudson, R. F.; Eisenstein, O.; Anh, N. T. *Tetrahedron* **1975**, *31*, 751. (b) DeFrees, D. J.; Bartmess, J. E.; Kim, K. J.; McIver, R. T., Jr.; Hehre, W. J. *J. Am. Chem. Soc.* **1977**, *99*, 6451. (c) Janousek, B. K.; Zimmerman, A. H.; Reed, K. J.; Brauman, J. I. *J. Am. Chem. Soc.* **1978**, *100*, 6142.
(34) Ingemann, S.; Nibbering, N. M. M. *J. Chem. Soc., Perkin Trans. 2* **1985**, 837.
(35) (a) Larson, J. R.; Epiotis, N. D. *J. Am. Chem. Soc.* **1981**, *103*, 410. (b) Epiotis, N. D.; Yates, R. L.; Bernardi, F.; Wolfe, S. *J. Am. Chem. Soc.* **1976**, *99*, 5435.
(36) Doncaster, A. M.; Walsh, R. *J. Chem. Soc., Faraday Trans. 1* **1976**, *72*, 2908.
(37) Davidson, I. M. T.; Hughes, K. J.; Ijadi-Maghsoodi, S. *Organometallics* **1987**, *6*, 646.

Hydrogen Atom Tunneling in the Thermal Tautomerism of Porphine Imbedded in a *n*-Hexane Matrix

Thomas J. Butenhoff and C. Bradley Moore*

Contribution from the Department of Chemistry, University of California, Berkeley, California 94720, and Materials and Chemical Sciences Division of the Lawrence Berkeley Laboratory, Berkeley, California 94720. *Received July 6, 1988*

Abstract: Rate constants and the kinetic isotope effect for the tautomerization of porphine imbedded in a *n*-hexane Shpol'skii matrix near 110 K have been measured with laser-induced fluorescence spectroscopy. A one-dimensional tunneling model calculation has been used to compare the feasibility of the synchronous and asynchronous hydrogen migration mechanisms. Only the asynchronous tunneling model is consistent with the rate constants and kinetic isotope effects measured near 110 K and near room temperature.

It has been established by both NMR[1] and X-ray crystallographic structure studies[2] that the inner hydrogens of free-base porphyrins are located on opposite pyrole rings (Figure 1). NMR studies on ring-substituted porphyrins have shown that the exchange of the inner hydrogens from one pair of nitrogens to the

* Address correspondence to this author at the University of California.

(1) Gust, D.; Roberts, J. D. *J. Am. Chem. Soc.* **1977**, *99*, 3637.
(2) Tulinsky, A. *Ann. N.Y. Acad. Sci.* **1973**, *206*, 47.

0002-7863/88/1510-8336$01.50/0

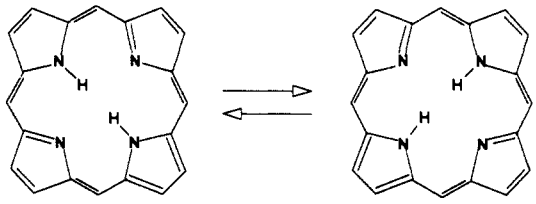

Figure 1. Tautomerism of free-base porphine (H_2P).

other is rapid at room temperature in both solution[3] and the solid state.[4] Several NMR studies have measured the kinetics of the hydrogen migration of various ring-substituted porphyrins to temperatures as low as 168 K[4-8] and no non-Arrhenius behavior has been observed.

At moderate and low temperatures, transition-state theory predicts linear Arrhenius curves, A^H/A^D ratios that are between 0.7 and 1.2, and $E_a^D - E_a^H$ values that do not exceed the zero-point energy differences of the initial states,[9] where A^H and E_a^H are the Arrhenius pre-exponential factor and the activation energy for the hydrogen migration reaction, and A^D and E_a^D are the Arrhenius parameters for the deuterium migration reaction. It has been established that the hydrogen migration in porphyrins occurs via tunneling based on the large values for $E_a^D - E_a^H$ and small A^H/A^D ratios measured for *meso*-tetraarylporphyrins.[10,11] However, there is uncertainty as to whether the hydrogens move synchronously[10] or asynchronously[12,13] during the reaction. The measurement of rate constants and kinetic isotope effects at low temperatures should help determine the mechanism. This investigation measured the kinetics for the thermal hydrogen migration in free-base porphine (H_2P) in the temperature range of 95 to 110.5 K and in the deuteriated free-base porphine (D_2P) in the range of 111.5 to 130 K. These rates are compared to the H_2P tautomerism rates measured near room temperature by Frydman et al.[14]

The porphine was incorporated in a *n*-hexane Shpol'skii matrix.[15,16] At 12 K, porphine occupies one major site in a *n*-hexane matrix[17] and two major sites in a *n*-hexane-d_{14} matrix. For each site, the porphine has two orientations, or tautomers, which differ by a 90° rotation in the plane of the molecule with respect to the crystal axes;[18] this rotation is equivalent to exchanging the two inner hydrogens from one pair of nitrogens to the other. The two tautomers have different crystal field effects which cause their $S_1 \leftarrow S_0$ absorptions to differ by about 100 cm^{-1}; the line widths of these transitions are about 3 cm^{-1}. The tautomer populations were probed by taking fluorescence excitation spectra of the $S_1 \leftarrow S_0$ 0–0 band. The tautomers do not thermally interconvert at 12 K, but irradiation of the 0–0 band of one tautomer photochemically converts it to the other tautomer of that site and vice versa.[19]

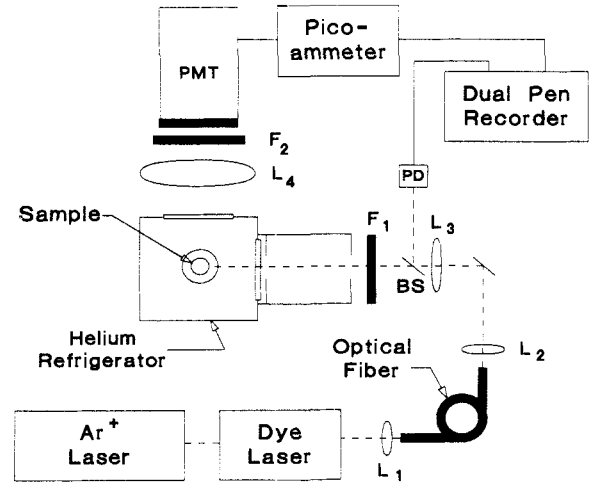

Figure 2. Schematic drawing of the apparatus used to take fluorescence excitation spectra: F_1, 10^{-3} neutral density filter; F_2, $\lambda_{pass} > 645$ nm filter; L, lens; BS, microscope slide beamsplitter; and PD, photodiode.

Experimental Section

A saturated solution of porphine (Porphyrin Products; used as purchased) in dry *n*-hexane (*n*-C_6H_{14}, Fluka chemicals, >99.7% pure; *n*-C_6D_{14}, MSD Isotopes, 99.3 atom % D; both were used as purchased) was sealed under vacuum in a sample cell. Deuteriated porphine, where the two inner hydrogen atoms are replaced with deuterium, was made by dissolving porphine in C_2H_5OD and then evaporating the solvent. This procedure was repeated with dry hexane to remove traces of ethanol.

Two types of sample cells were used in these experiments: a sealed tube and a paddle-shaped cell. The sealed tube had a 0.5 mm thick infrasil wall and a 4 mm outer diameter and was typically 15 mm long. The paddle-shaped cells were glassblown and are similar in design to those used by Shpol'skii.[20] They were cylindrical cells with 15 mm diameter, 1 mm thick fused silica windows, and a 1 mm path length; they were filled through a 4 mm outer diameter thick-walled tube that was attached to the side of the cell. The visible absorption spectrum of the samples was taken and the H_2P concentration was estimated to be 3×10^{-5} M.

The samples were fastened into copper blocks that were mounted in an Air Products Inc. Model CSA 202 closed cycle helium refrigerator. An internally referenced Air Products Model APD IC-1 proportional controller monitored and controlled the temperature of the sample. The proportional controller measured the emf from a KP vs iron-doped gold (0.7 atomic % doping) thermocouple, which was placed between the cold head and the copper block, and displayed the corresponding temperature on a dial that was read to ±0.5 K. The controller displayed the correct temperature for both an ice–water bath and liquid nitrogen; temperatures within this range were read from the dial without further calibration. The controller was used to vary the temperature of the sample between 12 and 150 K and maintained a desired temperature to ±1 K.

The porphine samples were probed by fluorescence excitation spectroscopy. Light from an argon ion pumped continuous wave dye laser was coupled out of an adjoining lab to the experiment by a multimode optical fiber. The dye laser (Spectra-Physics Model 375, Rhodamine 590 dye) had a bandwidth of 1 cm^{-1} and a typical output power of 30–60 mW. Typically, 8% of the laser light was tranmitted through the optical fiber. A small amount of the fiber output was reflected onto a photodiode for normalization of the dye laser power.

Figure 2 shows a schematic of the fluorescence excitation apparatus. A right angle geometry was used. A 6 cm diameter $f/1.1$ lens collected and focused the fluorescence through two Corning RG-645 filters (λ pass > 645 nm) and onto the cooled cathode of an RCA C31034 photomultiplier tube (PMT) housed at −30 °C in a Products for Research Inc. refrigerated housing. The current from the PMT was amplified by a picoammeter and recorded on a dual pen stripchart recorder. The stripchart simultaneously recorded the dye laser power for normalization.

The unattenuated laser power on the sample was ≈3 mW/cm^2. When probing the sample, the dye laser was attenuated with a 10^{-3} neutral

(3) Storm, C. B.; Teklu, Y.; Sokoloski, E. A. *Ann. N.Y. Acad. Sci.* **1973**, *206*, 631.
(4) Limbach, H. H.; Kendrick, R.; Yannoni, C. S. *J. Am. Chem. Soc.* **1984**, *106*, 4059.
(5) Hennig, J.; Limbach, H. H. *J. Chem. Soc., Faraday Trans. 2* **1979**, *75*, 752.
(6) Stilbs, P. *J. Magn. Reson.* **1984**, *58*, 152.
(7) Schlabach, M.; Wehrle, B.; Limbach, H. H.; Bunnenberg, E.; Knierzinger, A.; Shu, A. Y. L.; Tolf, B. R.; Djerassi, C. *J. Am. Chem. Soc.* **1986**, *108*, 3856.
(8) Crossley, M. J.; Field, L. D.; Harding, M. M.; Sternhell, S. *J. Am. Chem. Soc.* **1987**, *109*, 2335.
(9) Bell, R. P. *The Tunnel Effect in Chemistry*; Chapman and Hall: New York, 1980.
(10) Limbach, H. H.; Hennig, J.; Gerritzen, D.; Rumpel, H. *Faraday Discuss. Chem. Soc.* **1982**, *74*, 229.
(11) Eaton, S. S.; Eaton, R. G. *J. Am. Chem. Soc.* **1977**, *99*, 1601.
(12) Sarai, A. *J. Chem. Phys.* **1982**, *76*, 5554.
(13) Smedarchina, Z.; Siebrand, W.; Wildman, T. A. *Chem. Phys. Lett.* **1988**, *143*, 395.
(14) Frydman, L.; Olivieri, A. C.; Diaz, L. E.; Frydman, B.; Morin, F. G.; Mayne, C. L.; Grant, D. M.; Adler, A. D. *J. Am. Chem. Soc.* **1988**, *110*, 336.
(15) Shpol'skii, E. V. *Sov. Phys. Usp.* **1962**, *5*, 522.
(16) Shpol'skii, E. V. *Sov. Phys. Usp.* **1963**, *6* 411.
(17) Macfarlane, R. M.; Völker, S. *Chem. Phys. Lett.* **1980**, *69*, 151.
(18) van Dorp, W. G.; Soma, M.; Kooter, J. A.; van der Waals, J. H. *Mol. Phys.* **1974**, *28*, 1551.
(19) Völker, S.; van der Waals, J. H. *Mol. Phys.* **1976**, *32*, 1703.
(20) Shpol'skii, E. V. *Sov. Phys. Usp.* **1960**, *3*, 372.

density filter to avoid the photoconversion of the tautomers. The tautomer photoconversion caused from probing was measured by setting the dye laser to the 0–0 band of one tautomer and measuring the rate of the decay of the fluorescence signal. The fluorescence was fit to a single exponential decay[19] and the time constant was always greater than 3000 s. The laser was scanned 1 cm^{-1}/s which caused a calculated interconversion of ≤0.1% per spectrum. In practice, no interconversion was observed when taking spectra under probing conditions.

The kinetics experiment was started with the sample at 12 K. One of the tautomers was photochemically eliminated via prolonged irradiation in its 0–0 band. Because of hole-burning, the elimination of a tautomer had to be done by varying the laser frequency in steps over the entire 0–0 band of the tautomer to be erased. It typically took 10 to 20 min for H_2P and 1 h for D_2P to reduce the mole fraction of the undesired tautomer to under 0.06.

The sample was warmed from 12 K to the desired temperature; it took approximately 6 min to heat the sample from 12 to 110 K, though it only took about 2 min to heat from 90 K, where the migration of the hydrogens is virtually stopped on the time scale of the experiments, to 110 K. The temperature was maintained at least 30 min and then cooled to 12 K at which temperature its fluorescence excitation spectrum was taken. Cooling from 110 to 12 K took about 20 min, though once again, cooling to 90 K only took about 5 min. The experiment was repeated for several different temperatures for both H_2P in a *n*-hexane matrix and D_2P in a *n*-hexane-d_{14} matrix.

Data Analysis and Results

Figure 3 shows the fluorescence excitation spectra of the $S_1 \leftarrow S_0$ 0–0 band of H_2P (or D_2P) in a *n*-hexane matrix and in a *n*-hexane-d_{14} matrix. The site and tautomer labeling convention is that of Völker and van der Waals;[19] capital letters denote the site and a subscript of 1 or 2 denotes the two tautomers.

The porphine occupies one site in a *n*-hexane matrix; the absorption peaks for tautomers A_1 and A_2 were measured to be 609.9 and 613.7 nm, which agree well with the literature values.[17] Porphine occupies two sites in a *n*-hexane-d_{14} matrix which are labeled A and A′. The peaks at 613.7 and 613.3 nm are assigned to A_2 and A_2'; the peak at 609.7 nm is assigned to the unresolved A_1 and A_1' absorptions. When the red edge of the A_1–A_1' peak is irradiated with the laser, the intensity of A_2 increases with respect to A_2'; when the blue edge of the A_1–A_1' peak is irradiated, A_2' increases with respect to A_2.

The A site in *n*-hexane-d_{14} is probably the same as the A site in *n*-hexane. It is not known why there is a second site in the deuteriated hexane. The A′ site coalesces to the A site at temperatures above 40 K. At the temperatures of the thermal experiments, it is presumed that there is only one site in both types of hexanes and that the hexane sites are the same.

The tautomer populations are proportional to the integrated fluorescence peaks. The fluorescence peak area when all of the porphine is photochemically converted to one tautomer is equal, within the 4% experimental uncertainty, to the total intensity when all of the porphine is converted to the other tautomer. This establishes that the detection sensitivity is the same for both tautomers.

The kinetics of the porphine tautomerism can be described by

$$A_1 \underset{k_2}{\overset{k_1}{\rightleftharpoons}} A_2 \qquad (1)$$

where A_1 and A_2 are the two tautomers, and k_1 and k_2 are the rate constants for the forward and reverse reactions. The rate equation is

$$da_1/dt = -k_1a_1 + k_2a_2 \qquad (2)$$

where a_1 and a_2 are the mole fractions of tautomers 1 and 2. Remembering that $K_{eq} = k_1/k_2 = a_{2,eq}/a_{1,eq}$ and $a_1 + a_2 = 1$, the integrated rate equation can be written as

$$\ln (a_{2,eq} - a_2) = \ln (a_{2,eq} - a_{2,0}) - (k_1 + k_2)t \qquad (3)$$

where $a_{2,eq}$ is the equilibrium mole fraction of tautomer 2 and $a_{2,0}$ is the initial mole fraction of tautomer 2.

The equilibrium constant for H_2P in the *n*-hexane matrix was measured to be 2.44 at 108 K by allowing the thermal reaction to proceed for 48 h, which is equal to about 30 time constants.

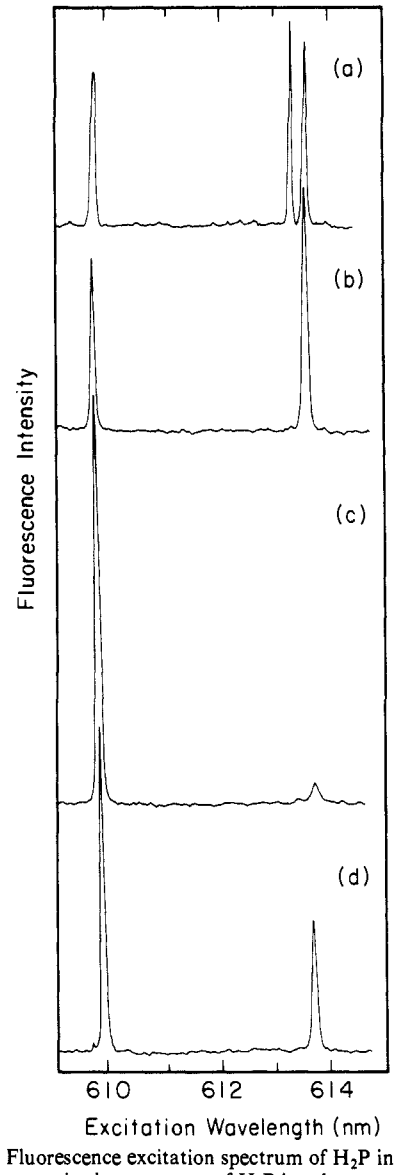

Figure 3. (a) Fluorescence excitation spectrum of H_2P in *n*-hexane-d_{14}. (b) Fluorescence excitation spectrum of H_2P in *n*-hexane. (c) Spectrum taken after photoconverting most of the porphine to the A_1 tautomer. (d) Spectrum shows the thermal tautomer conversion after 70 h at 95 K. All spectra were taken with the sample at 12 K and are not normalized for incident laser power.

The Gibbs free energy of reaction, ΔG, was calculated to be −67 cm^{-1} by using eq 4,

$$K_{eq} = \frac{k_1}{k_2} = \frac{a_{2,eq}}{a_{1,eq}} = \exp\left(\frac{-\Delta G}{k_B T}\right) \qquad (4)$$

where k_B is Boltzmann's constant. ΔG was assumed to be constant over the 16 deg temperature range of the experiment and the equilibrium constants for the other temperatures were calculated by using eq 4. The values for $a_{2,eq}$ at the other temperatures were derived from the equilibrium constants.

In a similar manner, the equilibrium constant was measured for D_2P in a *n*-hexane-d_{14} matrix at 126 and 129 K and ΔG was calculated to be 54 cm^{-1}. The equilibrium constant, as well as $a_{2,eq}$, was calculated for $T = 111.5$ K with eq 4.

The sums of the tautomerism rates, $k_1 + k_2$, at the different temperatures were determined from the slopes of the plots of $\ln (a_{2,eq} - a_2)$ vs time (see eq 3). The individual rates were determined by combining $k_1 + k_2$ with the equilibrium constant $K_{eq} = k_1/k_2$. Figure 4 shows some typical plots of $\ln (a_{2,eq} - a_2)$ vs time; Table I lists the rate constant results. The uncertainty in the measurement of $a_{2,eq}$ is included in the error bar of each $\ln (a_{2,eq} - a_2)$ point. The quoted uncertainties in the $k_1 + k_2$ values

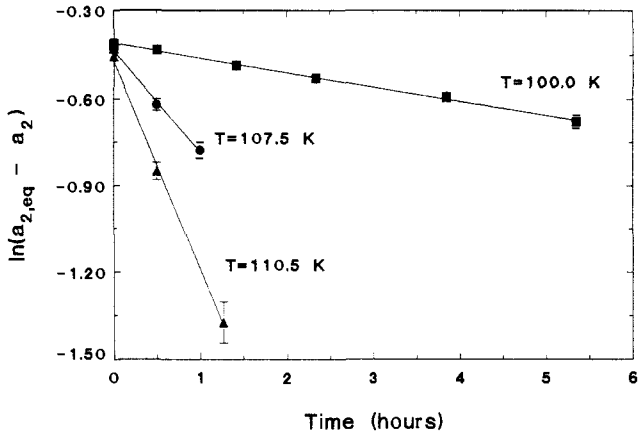

Figure 4. Obtaining tautomerism rates from fluorescence intensities: H_2P in *n*-hexane.

Table I. Porphine Tautomerism Rate Constants

T (K)	$k_1 + k_2$ (10^{-6} s^{-1})	a_2,eq/a_1,eq = k_1/k_2	k_1 (10^{-6} s^{-1})
	H_2P		
110.5[a]	200 ± 18	2.39[d]	141 ± 13
108.0[a]	170 ± 40	2.44[c]	121 ± 29
107.5[a]	96 ± 11	2.45[d]	68 ± 8
100.0[b]	13.6 ± 1.7	2.62[d]	9.8 ± 1.2
95.0[b]	2.1 ± 0.2	2.76[d]	1.5 ± 0.2
	D_2P		
129.0[a]	37 ± 15	1.82[c]	24.0 ± 9.7
126.0[a]	28.9 ± 5.5	1.85[c]	18.6 ± 3.6
111.5[b]	0.82 ± 0.28	2.01[d]	0.55 ± 0.19

[a] ±0.5 K. [b] ±1 K. [c] Measured value. [d] Calculated value.

Table II. Porphine Arrhenius Parameters

	temp range (K)	log (A/s^{-1})	E_a (kJ/mol)
H_2P	95–110.5	8.8 ± 1.8	26.8 ± 3.7
D_2P	111.5–129	6.1 ± 1.7	26.5 ± 3.9

are determined by the extreme maximum and minimum sloped lines that fit the data points plus error bars. The averages of k_1 and k_2 were used to determine the Arrhenius parameters for H_2P and D_2P that are listed in Table II. A weighted least-squares fitting program was used and the quoted uncertainties represent two standard deviations.

Discussion

Although it is well established that the porphyrin tautomerism occurs via tunneling, there is uncertainty as to whether the hydrogens move synchronously[10] or asynchronously[12,13] during the reaction. To address this problem, the rates and kinetic isotope effect reported here for the porphine tautomerism measured in a *n*-hexane matrix near 110 K are compared with the rates and expected isotope effect of H_2P in solution near room temperature that were measured by Frydman et al.[14] The effect of the *n*-hexane matrix on the tautomerism rate is expected to be small for two reasons: Shpol'skii matrices only weakly interact with the guest molecules,[16] and crystalline H_2P tautomerism rates are within a factor of 3 of the rates measured in solution.[21]

In the synchronous migration the reaction coordinate corresponds to the simultaneous migration of the two inner hydrogens. The potential energy along this path is a symmetrical double-well potential, or a nearly symmetrical double well in the case of crystalline porphine or porphine imbedded in the *n*-hexane matrix. The reduced mass for this process in H_2P is 2 g/mol.

Figure 6 shows a schematic of the potential energy diagram for the asynchronous process. In this model a single hydrogen tunnels from a potential well with hydrogens on opposite nitrogens to a well with hydrogens on adjacent nitrogens. For hydrogen

(21) Wehrle, B.; Limbach, H. H.; Köcher, M.; Ermer, O.; Vogel, E. *Angew. Chem., Int. Ed. Engl.* **1987**, *26*, 934.

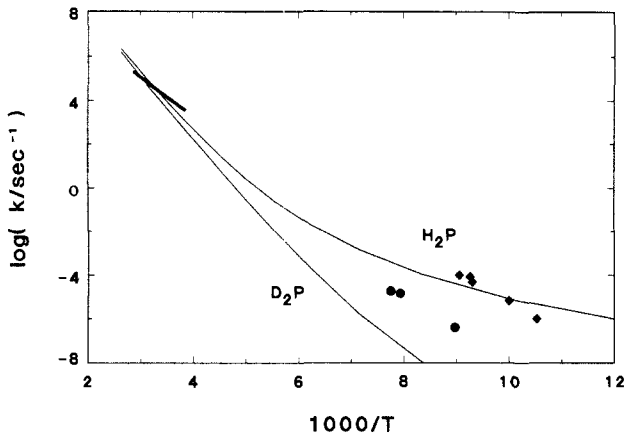

Figure 5. H_2P and D_2P Arrhenius plots: the solid diamonds and circles are the rates measured for H_2P and D_2P in this work; the error bars are smaller than the point size. The thick line is the H_2P Arrhenius curve from ref 14. The two curves are the tunneling calculation assuming synchronous migration of the inner hydrogens: the value of L is 1.23 Å, $A_s = 1.0 \times 10^{14}$ s^{-1}, and $V_0(H_2P) = V_0(D_2P) = 4850$ cm^{-1}.

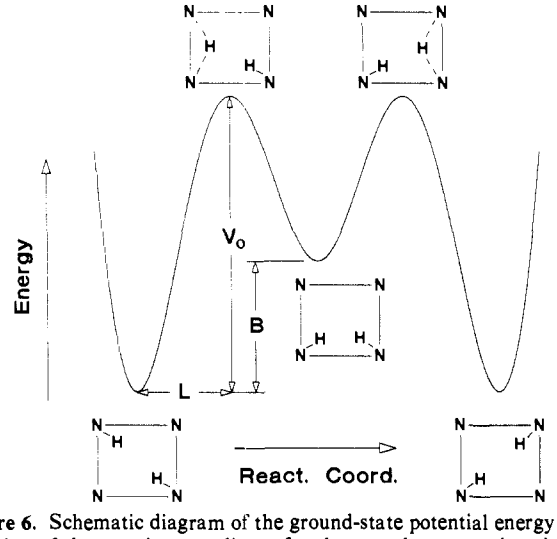

Figure 6. Schematic diagram of the ground-state potential energy as a function of the reaction coordinate for the asynchronous migration in H_2P.

migration, the reduced mass is 1 g/mol. The kinetics can be described by

$$A \underset{k_{BA}}{\overset{k_{AB}}{\rightleftharpoons}} B \xrightarrow{k_{BC}} C \qquad (5)$$

where A is the reactant, B the intermediate, and C the product. If the steady-state approximation is made for the intermediate, the rate of reactants forming products is

$$k = \frac{k_{AB}k_{BC}}{k_{BA} + k_{BC}} \qquad (6)$$

The approximation is made that the energy for both tautomers is equal; then, for H_2P and D_2P, k_{BA} is equal to k_{BC}. The net rate of reactants forming products is equal to half the rate of the reactants going to the intermediate.

A one-dimensional tunneling model is used to compare the feasibility of the synchronous and asynchronous migration mechanisms. The rate of the reaction can be described by[9]

$$k = A_s Q_t \exp\left(-\frac{V_0}{k_B T}\right) \qquad (7)$$

where A_s is the classical pre-exponential factor, V_0 is the barrier height, and Q_t is the tunneling correction for a one-dimensional barrier. The tunneling correction for a Boltzmann distribution of reactant states is[9]

$$Q_t = \frac{\exp\left(\frac{V_0}{k_B T}\right)}{k_B T} \int_0^\infty G(E) \exp\left(-\frac{E}{k_B T}\right) dE \qquad (8)$$

where E is the energy of the reactant state and $G(E)$ is the barrier permeability. To be exact, the integral in eq 8 should be replaced by a sum over discreet reactant energies, but Sarai has shown that low-frequency skeletal modes are coupled to the reaction coordinate.[12,22] Even at 100 K, the average energy of the molecules undergoing the reaction is about 2000 cm^{-1} ($E_a \approx 2200$ cm^{-1}) above their zero-point energy. Therefore, making the approximation of a continuous distribution of reactant states is reasonable.

A generalized Eckart barrier is used to model the barrier:

$$V(x) = \frac{Ay}{(1+y)^2} + \frac{By}{(1+y)}, \; y = \exp(2\pi x/L) \qquad (9)$$

The Eckart barrier parameters are shown in Figure 6. The barrier height with respect to the energy zero of the reactant is given by

$$V_0 = (A + B)^2/4A \qquad (10)$$

B is the energy difference between the product and the reactant. L varies the width of the barrier; $x \approx -L$ corresponds to the bottom of the reactant well, and $x \approx L$ corresponds to the product well minimum. The Eckart barrier permeability is given by[9]

$$G(E) = \frac{\sinh^2(\frac{1}{2}kL(1+\Delta)) - \sinh^2(\frac{1}{2}kL(1-\Delta))}{\sinh^2(\frac{1}{2}kL(1+\Delta)) + \cosh^2\left(\frac{\pi}{2}\left[\frac{8mL^2A}{(2\pi\hbar)^2} - 1\right]^{1/2}\right)} \qquad (11)$$

where $k = (2mE)^{1/2}/\hbar$ and $\Delta = (1 - B/E)^{1/2}$.

A symmetrical Eckart barrier is used to calculate the tunneling correction for the synchronous migration; i.e., $B = 0$ in eq 9, 10, and 11. It is assumed that the classical pre-exponential factor is equal to the N–H stretching frequency, which is 1.0×10^{14} s^{-1}. For a given value of L the barrier height is varied until the calculated rate is equal to the measured rate at 300 K. Figure 5 shows the calculation for $L = 1.23$ Å. For values of L less than this value, the calculated rates at 100 K are higher than the measured rates. D_2P rates are calculated by changing the tunneling mass from 2 to 4 g/mol. The barrier for D_2P will be greater than or equal to the barrier for H_2P because of zero-point energy differences; the barrier is varied within this constraint to reproduce the data measured at 111 K as well as possible. The kinetic isotope effect for porphine is expected to be about the same as for tetraarylporphyrins, which is about 10 at 300 K;[5,11] the calculated isotope effect at 300 K is only 1.9.

A lower pre-exponential factor of 5.0×10^{12} s^{-1} is used for a second set of calculations. Values of L less than 1.28 Å give rates that are too large at 100 K. With L equal to 1.28 Å, the calculated kinetic isotope effect at 300 K is only 1.7, which is much lower than expected. If the D_2P barrier height is increased until the calculated isotope effect at 300 K is 10, then the predicted isotope effect at 111 K is about 600 times larger than the measured isotope effect. The synchronous migration tunneling model cannot reproduce the measured H_2P rates and the kinetic isotope effects at both low and high temperatures with reasonable classical pre-exponential factors.

An asymmetric Eckart barrier, with $B > 0$, is used to calculate the tunneling correction for the asynchronous migration. For a given value of L and classical pre-exponential factor, the barrier height is varied to match the measured H_2P rate at 300 K. Then B, which is the endothermicity of the intermediate with respect to the reactant, is varied to reproduce the measured rate at 100 K. To calculate the D_2P rates, the tunneling mass is changed from 1 to 2 g/mol and the barrier height is allowed to be greater than or equal to the barrier height for H_2P. Figure 7 shows a typical good fit. Good fits are obtained with an A_s of 1.0×10^{14} s^{-1} and values of L of 0.78 to 1.05 Å; V_0 for H_2P varies from 5620 to 5050 cm^{-1}, B from 1890 to 1670 cm^{-1}, and the kinetic isotope effect at 300 K from 19 to 5. D_2P barrier heights are within 70 cm^{-1} of the H_2P barrier heights. The calculated imaginary frequencies that correspond to the curvature at the top of the H_2P barriers vary between 2144 and 1534 cm^{-1}.

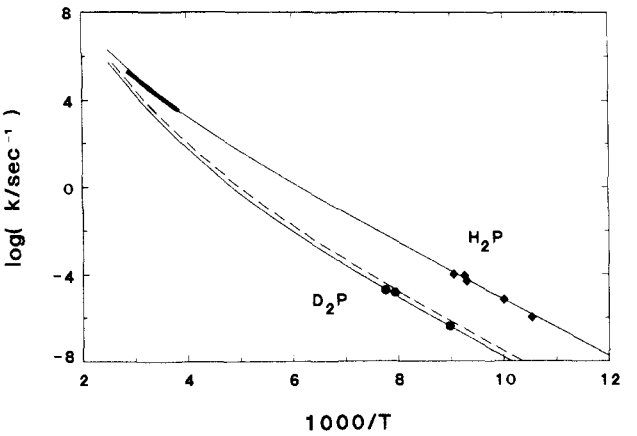

Figure 7. The asynchronous migration tunneling calculations: the experimental points are the same as in Figure 5. The solid curves are the calculations for H_2P and D_2P; the dashed curve is the calculation for HDP. The value for L is 0.84 Å, $A_s = 1.0 \times 10^{14}$ s^{-1}, $V_0(H_2P) = 5450$ cm^{-1}, $V_0(D_2P) = 5470$ cm^{-1}, and $B = 1890$ cm^{-1}.

A pre-exponential factor of 5.0×10^{12} s^{-1} is used for a second set of calculations. The biggest effect on the barrier parameters is on the barrier height, V_0. Good fits are obtained with values of L of 0.78 to 0.99 Å; V_0 for H_2P varies from 4600 to 4400 cm^{-1}, B from 1960 to 1770 cm^{-1}, and the kinetic isotope effect at 300 K from 21 to 5. The D_2P barrier heights are 330 to 110 cm^{-1} greater than the barrier heights for H_2P. The calculated imaginary frequencies that correspond to the curvature at the top of these H_2P barriers vary between 1853 and 1425 cm^{-1}; these frequencies seem reasonable.

The tautomerism rate for the mono-deuteriated porphine (HDP) has not been measured, but the rate for the mono-deuteriated tetraphenylporphyrin was found to be about the same as that for the di-deuteriated tetraphenylporphyrin.[10] The rate for HDP is calculated with the asynchronous tunneling model. k_{AB} in eq 6 corresponds to the H atom migrating to form the intermediate and k_{BC} corresponds to the D atom migrating to form the product. The H_2P barrier height is used for the H atom migration barrier height and the D_2P barrier height is used for the D atom migration barrier height. Figure 7 shows a typical result; as can be seen, the HDP Arrhenius curve is close to the D_2P curve throughout the temperature range, which is consistent with the experimental results for the mono-deuteriated tetraphenylporphyin.

A reduced mass of 3 g/mol is used to calculate the HDP rate with the synchronous tunneling model. The calculated HDP rate is approximately the geometric mean of the H_2P and D_2P rates, which is not consistent with the results for tetraphenylporphyrin.

Conclusion

The rate of tautomerism and kinetic isotope effect of free-base porphine imbedded in a *n*-hexane matrix have been measured near 110 K and the rates have been compared with previously published rates measured by NMR in solution near room temperature. A one-dimensional tunneling model has been used to fit the Arrhenius curves.

Both the synchronous and asynchronous migration one-dimensional tunneling model can reproduce the rates and kinetic isotope effect for the tautomerism in porphyrins near room temperature, but only the asynchronous migration tunneling model can also reproduce the rates and isotope effect of porphine near 110 K. The synchronous migration tunneling model predicts Arrhenius plots that are too curved and kinetic isotope effects at

(22) Sarai, A. *Chem. Phys. Lett.* **1981**, *83*, 50.

110 K that are too large. These results are in qualitative agreement with Smedarchina et al.'s golden rule tunneling calculation for tetraphenylporphyrin.[13]

Considering the simplicity of the tunneling model, the barrier parameters cannot be taken too literally. Reasonable fits can be obtained for barrier heights of 4400–5700 cm^{-1}, depending on the classical pre-exponential factor. The porphine isomer with the inner hydrogens on adjacent nitrogens has a calculated energy of 1670–1960 cm^{-1} above the energy of the isomer with hydrogens on opposite nitrogens. The calculated rate for the mono-deuteriated porphine is very close to the rate for the di-deuteriated porphine, which is consistent with experimental results for tetraphenylporphyrin.[10]

Acknowledgment. We thank Hans Limbach for helpful discussions and encouragement. This research was supported by the Director, Office of Energy Research, Office of Basic Energy Sciences, Chemical Sciences Division of the U.S. Department of Energy under Contract No. DE-AC03-76SF00098. T.J.B. acknowledges support from the National Science Foundation in the form of a predoctoral fellowship.

Registry No. Porphine, 101-60-0; deuterium, 7782-39-0.

Nephelauxetic Effect in Paramagnetic Shielding of Transition-Metal Nuclei in Octahedral d^6 Complexes

Nenad Juranić

Contribution from the Department of Chemistry and Physical Chemistry, Faculty of Sciences, University of Belgrade, P.O. Box 550, 11001 Belgrade, Yugoslavia. *Received February 1, 1988*

Abstract: For transition metals, using reliable d electron radial wave functions, it was calculated that the d electron radial parameters, B_{Racah} and $\langle r_d^{-3}\rangle$, are equally influenced by change in the d-orbital occupancy. On this basis, introduction of the first power of the nephelauxetic ratio into the paramagnetic shielding term of octahedral d^6-complex transition-metal nuclei is justified. Interpretations of rhodium NMR chemical shifts in rhodium(III) complexes were analyzed.

In the recent interpretation of metal NMR chemical shifts in octahedral d^6 transition metal complexes,[1] the paramagnetic shielding term (σ^p) has been expressed by the ligand field parameters in the following way:

$$\sigma^p = -8\frac{\mu_0{\mu_B}^2}{\pi}\langle r_d^{-3}\rangle_F\frac{\beta_{35}}{\Delta E} \qquad (1)$$

(where μ_0 is the vacuum permeability, μ_B the Bohr magneton, $\langle r_d^{-3}\rangle_F$ the free-ion(atom) expectation value of d electron inverse cube distance, β_{35} the nephelauxetic ratio, and ΔE the energy of the $^1A_{1g}\leftarrow{}^1T_{1g}$ electronic transition). Some arguments for incorporation of the nephelauxetic ratio into the paramagnetic shielding term, based on molecular orbital analysis of the covalency effects, have been put forward.[2] However, the general validity of the proposed relationship has been questioned by Bramley et al.,[3] since they would rather expect the third power of the nephelauxetic parameter to be incorporated in the paramagnetic shielding term. They suggested that rhodium chemical shifts in rhodium(III) complexes are in accordance with that expectation. Therefore, I undertook further investigation of the theoretical foundation of eq 1, the results of which are presented here.

Results

Ramsey's theory of nuclear paramagnetic shielding, applied to a metal with d^6 configuration in a strong octahedral ligand field,[4,5] leads, in the molecular orbital formulation,[2,6] to the expression:

$$\sigma^p = -\frac{\mu_0 e^2}{4\pi m^2}\frac{\langle e_g|\sum_k l_{z,k}|t_{2g}\rangle\langle t_{2g}|\sum_k l_{z,k}r_k^{-3}|e_g\rangle}{\Delta E(^1A_{1g}\leftarrow{}^1T_{1g})} \qquad (2)$$

(where l_z is orbital angular momentum operator). Molecular orbitals $e_g(t_{2g}^5e_g:{}^1T_{1g})$ and $t_{2g}(t_{2g}^6:{}^1A_{1g})$, which in the ionic limit are reduced to the metal $d_{x^2-y^2}$ and d_{xy} orbitals, respectively, contain information on the metal–ligand bond covalency. As a measure of the impact of covalency on the paramagnetic shielding term, the following ratio may be introduced:[2,7]

$$\eta_{\sigma\pi} = \frac{\langle e_g|\sum_k l_{z,k}|t_{2g}\rangle\langle t_{2g}|\sum_k l_{z,k}r_k^{-3}|e_g\rangle}{\langle d_{x^2-y^2}|\sum_k l_{z,k}|d_{xy}\rangle\langle d_{xy}|\sum_k l_{z,k}r_k^{-3}|d_{x^2-y^2}\rangle} \qquad (3)$$

which allows eq 2 to be put into the form:

$$\sigma^p = -8\frac{\mu_0{\mu_B}^2}{\pi}\langle r_d^{-3}\rangle_F\frac{\eta_{\sigma\pi}}{\Delta E} \qquad (4)$$

The theoretical foundation of eq 1 depends on whether the covalency ratio $\eta_{\sigma\pi}$ in eq 4 could be replaced by the nephelauxetic ratio β_{35}.

One may compare these two ratios by expressing relevant molecular orbitals as a linear combination of the corresponding atomic orbitals and, under the assumption of a small admixing of ligand into metal orbitals, obtain for $\eta_{\sigma\pi}$:[2]

$$\eta_{\sigma\pi} = a_\sigma{}^2a_\pi{}^2(\langle r_d^{-3}\rangle_C/\langle r_d^{-3}\rangle_F)$$

or for the nephelauxetic ratio:[8,9]

$$\beta_{35} = a_\sigma{}^2a_\pi{}^2(B_C/B_F)$$

(1) (a) Juranić, N. *Inorg. Chem.* **1980**, *19*, 1093. (b) Juranić, N. *Inorg. Chem.* **1985**, *24*, 1599. (c) Juranić, N. *J. Magn. Reson.* **1987**, *71*, 144.
(2) Juranić, N. *Inorg. Chem.* **1983**, *22*, 521.
(3) Bramley, R.; Brorson, M.; Sargenson, A. M.; Schäffer, C. F. *J. Am. Chem. Soc.* **1985**, *107*, 2780.
(4) Griffith, J. S.; Orgel, L. E. *Trans. Faraday Soc.* **1957**, *53*, 601.
(5) Freeman, R.; Murray, G. R.; Richardson, R. E. *Proc. R. Soc. London, Ser. A* **1957**, *242*, 455.
(6) Walstedt, R. E.; Wernick, J. M.; Jaccarino, V. *Phys. Rev.* **1967**, *162*, 301.

(7) Note also that:

$$\eta_{\sigma\pi} = k_{\sigma\pi}\frac{\langle t_{2g}|\sum_k l_{z,k}r_k^{-3}|e_g\rangle}{\langle d_{xy}|\sum_k l_{z,k}r_k^{-3}|d_{x^2-y^2}\rangle} \sim k_{\sigma\pi}{}^2\frac{\langle r_d^{-3}\rangle_C}{\langle r_d^{-3}\rangle_F}$$

where $k_{\sigma\pi}$ is the orbital angular momentum reduction factor: Stevans, K. W. H. *Proc. R. Soc. London, Ser. A* **1953**, *219*, 542.
(8) Fenske, R. F.; Coulton, K. G.; Radtke, D. D.; Sweeney, C. C. *Inorg. Chem.* **1966**, *5*, 960.
(9) Jørgensen, C. K. *Prog. Inorg. Chem.* **1962**, *4*, 73; *Struct. Bonding (Berlin)* **1966**, *1*, 3; *Inorg. Chim. Acta Rev.* **1968**, *2*, 65.

0002-7863/88/1510-8341$01.50/0